CFD Investigation of the Effect of Water Depth on Manoeuvring Forces on Inland Ships

Guido Oud[1,*] **and Antoine Bedos**[2]

[1]Maritime Research Institute Netherlands (MARIN)
Wageningen, The Netherlands
Research & Development
e-mail: g.oud@marin.nl

[2]Maritime Research Institute Netherlands (MARIN)
Wageningen, The Netherlands
Ships Department
e-mail: a.bedos@marin.nl

[*] Corresponding author: Guido Oud, g.oud@marin.nl

ABSTRACT

As part of a research program focusing on shallow-water manoeuvring of inland ships, a set of model tests is reproduced using CFD techniques. The aim of this study is to investigate the capability of MARIN's CFD software to predict manoeuvring forces and moments in shallow-water conditions using standardised procedures. The test matrix features small drift angles at different speeds and water depths with under-keel clearances between 20% and 100%. The computed hydrodynamic loads on the hull as well as the squat of the ship are compared with experimental results.

Keywords: CFD; shallow water; manoeuvring; basin tests; inland shipping

NOMENCLATURE

B	Ship breadth [m]
C_b	Block coefficient [-]
F_n	Froude number [-]
F_{n_h}	Depth Froude number [-]
h	Water depth [m]
L_{pp}	Length between perpendiculars [m]
N	Yaw moment [Nm]
Re	Reynolds number [-]
S	Blockage factor [-]
T	Ship draught (at rest) [m]
V	Sailing speed [m s^{-1}]
V_{cr}	Critical channel speed [m s^{-1}]
X	Surge force [N]
Y	Sway force [N]
β	Drift angle [deg]
Δ	Ship volumetric displacement [m^3]
ρ	Water density [kg m^{-3}]
θ	Pitch angle [deg]
CFD	Computational Fluid Dynamics
RANS	Reynolds-averaged Navier-Stokes
UKC	Under-keel clearance

1 INTRODUCTION

In 2019 Rijkswaterstaat and MARIN launched a joint research project on shallow-water effects. The study, made critical by the increasing occurrence of low water levels in Dutch rivers, is aimed at developing simulation models to investigate the effect of extreme shallow-water conditions on the manoeuvring performance of inland ships. Sailing in shallow water exacerbates the effect of disturbances to hull forces, for example due to an uneven riverbed geometry, and thereby impacts the manoeuvrability of ships. Due to the complexity of the underlying physics, more insight and experience are needed to be able to derive accurate mathematical models for shallow-water manoeuvring. Such models can then be used to provide advice and recommendations to shipping- and waterway authorities.

To that end, MARIN performed a substantial set of model tests over the last years to measure hull forces in shallow-water conditions on a typical inland vessel. Captive tests under drift were carried out at various sailing speeds and water depths, down to an under-keel clearance (UKC) of 10% of the draught.

Within the research project, resources were allocated to use some of the available experimental results as validation material for a restricted Computational Fluid Dynamics (CFD) investigation in order to examine the capability of MARIN's in-house viscous-flow solver ReFRESCO. A set of experiments was reproduced using CFD techniques, and the computed hydrodynamic loads were compared to model test measurements. Several numerical techniques were investigated in the course of the program, such as accurate free-surface modelling and the importance of squat modelling. This investigation did not include a refinement study as commonly used in numerical studies. Instead, the presented results are obtained using standardised procedures developed from experience within MARIN (for instance from Toxopeus et al. (2013)). Consequently, the results do not constitute a formal validation in numerical sense (which would require said refinement studies to determine uncertainties), but merely provide insights in ReFRESCO's ability to simulate shallow-water cases using MARIN's standardised practices. Comparison between numerical and experimental results are done on a qualitative level as much as possible, with the focus on capturing trends observed in the experiments. Possible sources of uncertainty (both in CFD and model test) that were identified are also presented.

Section 2 briefly presents the model tests and introduces the matrix of simulations. Section 3 provides details on the numerical simulations that have been performed, and in section 4 the CFD results are presented and analyzed. Finally, section 5 summarises the findings of this study.

2 TEST CASE: PURE DRIFT IN SHALLOW-WATER CONDITIONS

To compare experimental and numerical results of hull forces, a set of captive pure drift tests was selected. In these tests, the ship model is towed along the basin at a constant speed, and the forces and moments applied to the hull are recorded. The ship model is free to heave and pitch in order to account for the squat effect experienced by the hull in the confined shallow-water conditions.

2.1 Ship geometry

The ship considered in this study is a representative 110m inland ship (class Va), conventionally fitted with a single propeller and two fishtail-type rudders, in full-load condition. Table 1 indicates the main characteristics of the ship.

The ship model was manufactured at a scale ratio of 1:18. In the present study, only the bare-hull configuration is considered. Although experiments with appendages were performed, including them in the CFD investigation was deemed beyond the research scope. The model featured sand strips at the fore-shoulder to trigger turbulence around the hull and limit scale effects. An impression of the ship geometry as used in the CFD calculations is shown in figure 1.

Table 1. Main characteristics of the inland ship.

Dimension	Notation	Value (full scale)	Value (model scale)
Length between perpendiculars	L_{pp}	110.0 m	6.111 m
Breadth	B	11.4 m	0.633 m
Draught (at rest)	T	3.5 m	0.194 m
Displacement	Δ	3876.05 m^3	0.665 m^3
Block coefficient	C_b	0.883 [-]	0.883 [-]

(a) Starboard view of the hull

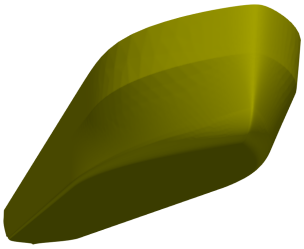

(b) View of the bow

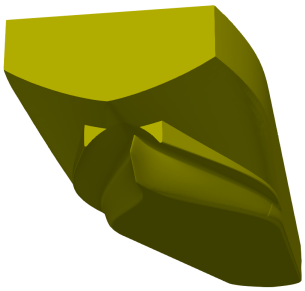

(c) View of the stern

Figure 1. Geometry of the inland ship used in both experiments and numerical computations.

2.2 Pure drift motions

This study includes a total of 18 conditions: three drift angles, three water depths, and two sailing speeds. One set of tests is performed at a constant sailing speed for all water depths, while the sailing speed of the second set follows from a constant fraction of the critical canal speed V_{c_r} (Römisch, 1989) defined as:

$$V_{c_r}(h, S) = \sqrt{gh}\left[2\sin\left(\frac{\arcsin(1-S)}{3}\right)\right]^{1.5}, \tag{1}$$

with S the blockage factor of the ship in the basin, h the water depth and g the gravitational acceleration. A summary of all cases is shown in table 2.

Table 2. CFD test matrix.

Depth-to-draught ratio h/T [-]	Drift angle β [deg]	Froude No. F_n [-]	Depth Froude No. F_{n_h} [-]	Speed ratio V/V_{c_r} [-]	Reynolds No. Re [-]
2.0	$0, -2, -6$	0.140	0.553	0.67	$6.6 \cdot 10^6$
	$0, -4, -10$	0.085	0.335	0.56	$4.0 \cdot 10^6$
1.4	$0, -2, -6$	0.112	0.529	0.67	$5.3 \cdot 10^6$
	$0, -4, -10$	0.085	0.401	0.50	$4.0 \cdot 10^6$
1.2	$0, -2, -6$	0.101	0.519	0.67	$4.8 \cdot 10^6$
	$0, -4, -10$	0.085	0.433	0.40	$4.0 \cdot 10^6$

The Froude number F_n and the depth Froude number F_{n_h} are defined as follows:

$$F_n = \frac{V}{\sqrt{gL_{pp}}}, \qquad F_{n_h} = \frac{V}{\sqrt{gh}}, \tag{2}$$

with V the sailing speed, and the Reynolds number Re follows from:

$$Re = \frac{VL_{pp}}{\nu}, \tag{3}$$

with ν the fresh water kinematic viscosity.

2.3 Model tests

MARIN's shallow-water basin was used to perform a dedicated set of experiments. The basin's length and width are 220m and 15.8m, respectively, with an adjustable water level up to 1.1m. This corresponds to a blockage factor S of 2.0% and 3.3% when sailing straight ahead at a water depth-to-draught ratio of 2.0 and 1.2, respectively. Figure 2 gives an impression of the basin during operations. The test matrix presented in table 2 is a subset of a larger testing program used to produce input for mathematical models for sailing in shallow-water conditions, and additionally providing experimental validation material for numerical simulations.

Figure 2. MARIN's shallow-water basin.

In addition to the tests described in the present study, the experimental project includes test at various speeds and drift angles. Furthermore, captive model tests with an appended model were performed (1 ducted propeller, 2 rudders). These results are not relevant for the current research question, but can be used in following studies for more advanced numerical simulations.

3 NUMERICAL MODELLING

All calculations performed in this study are performed with MARIN's proprietary CFD software ReFRESCO (ref). Many modelling considerations that are specifically relevant for shallow-water conditions have been investigated in previous studies. Examples are the simulation of the free surface (either as a horizontal symmetry plane (i.e. no waves) or using a two-phase flow solution), choice of boundary conditions (in particular for the bottom of the domain) and the size of the computational

domain (to remove boundary influences). The experience obtained from these studies has been used in the formation of a standardized work flow for simulations which is showing an increasing use due to growing commercial interest in shallow-water simulations. The numerical work in this study is produced using the in-house work flow with as little further tuning as possible.

3.1 Ship motion

In the simulations, the ship is held in a captive setup and sails at forward speed at a constant drift angle. In half of the cases (with constant speed ratio), the ship is free to trim and sink, in the other half (with constant speed) the squat is imposed (i.e. fixed from the beginning) based on the values from the basin tests. Although free squat motion is the closest approximation of reality, it is significantly more complex (and thus expensive) computationally than pre-imposed squat. Both techniques are applied to analyze their accuracy.

Mesh deformation is used to model the dynamic squat behaviour of the ship as well as to impose an initial drift angle so that a single topology can be used per water depth. The deformation employs radial basis functions to interpolate the displacement of the boundary nodes to the internal mesh (Rendall and Allen, 2009). The selection of the boundary nodes is optimized through the use of a greedy algorithm, and the resulting system of equations for the interpolation coefficients is solved using an efficient direct solver.

The trim and sinkage of the ship are determined at each time step by solving a subset of the equations of motion for a rigid body $\mathbf{M}\ddot{\mathbf{x}} = \mathbf{F}_{\text{hydro}}$, thereby mimicking the allowable degrees of freedom of the experiments. Here $\mathbf{M} \in \mathbb{R}^{6\times6}$ is the mass matrix, comprising the mass and inertia moments of the ship, $\mathbf{x} \in \mathbb{R}^6$ the vector containing the translations and rotations and $\mathbf{F}_{\text{hydro}} \in \mathbb{R}^6$ the vector with the computed hydrodynamic loads. Internal damping can be taken into account but is not included in this study. Under-relaxation can be applied when high-frequency non-physical oscillations are observed.

Derived from experience with resistance calculations in deep water, simulations involving free motion of a ship are considered to have finished when the equation of motion is converged in time, i.e. when a steady-state solution of the motion vector has been obtained. In shallow-water conditions, however, it was found that the existence of such a steady-state solution is not guaranteed, especially in extremely shallow water conditions. In such cases, where the ship movement becomes highly oscillatory and erratic, the stop criterion follows from statistical methods (Brouwer et al., 2019).

3.2 Computational mesh

The computational grids are constructed using the meshing software Hexpress. The hexahedral meshes are generated using automated scripting procedures that are based on grid generation experience within MARIN (Crepier, 2017). A small set of primary variables, such as ship geometry, sailing velocity and the presence of waves is used as input to create optimized meshes with specified resolution where needed while keeping the total number of cells to a minimum for performance. Local mesh refinement is applied close to the ship near the bow and the stern as shown in figures 3c and 3d, as well as in normal direction on the domain bottom and side walls. Additional refinement, derived from theoretical predictions, is placed around the free surface level to capture a potential wave pattern, as shown in figures 3a and 3b. Based on the input values, a certain cell density per expected wave length or height is guaranteed. Furthermore, refinement around the free surface level is applied to reduce smearing of the water-air interface (a known issue in algebraic Volume-of-Fluid algorithms, particularly in combination with hanging nodes in the mesh). On top of that, adaptive mesh refinement is used during the calculations for increased efficiency. The adaptive refinement is based on thresholds in fluctuations of the pressure Hessian and the air volume fraction. Finally, additional mesh refinement is applied in the normal direction to the ship surface and the bottom of the domain to fully resolve the boundary layer by keeping y^+ values sufficiently small. The number of volumetric cells for the

computations generally lies around 16 million (complete domain) after the last adaptive refinement step (although symmetry is exploited where possible so that only half the domain is used). The geometry of the ship is captured by approximately 250 thousand surface cells.

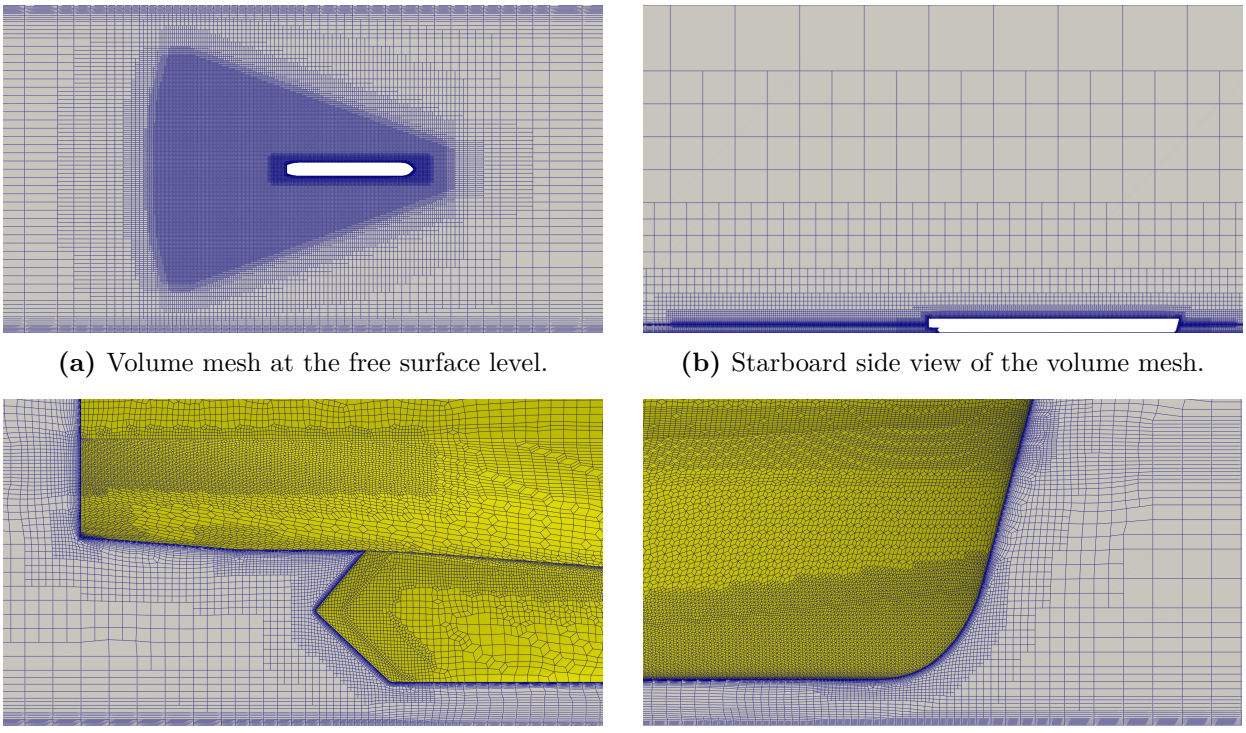

(a) Volume mesh at the free surface level.

(b) Starboard side view of the volume mesh.

(c) Surface mesh at the stern.

(d) Surface mesh at the bow.

Figure 3. Impression of the volume mesh (top row) and surface mesh (bottom row) typically used in the CFD calculations for $h/T = 1.2$.

3.3 Orientation of the motions

The positive orientation of ship translations (x, y and z) and their respective time derivatives (u, v and w) as used in this paper are shown in figure 4. A right-handed coordinate system is used with the z-axis pointing upwards, the y-axis pointing towards port and the origin situated at midship at free surface level. The drift angle β is defined as the angle between u and the sailing velocity $V := \sqrt{u^2 + v^2}$ as:

$$\beta := \arctan \frac{v}{u}. \tag{4}$$

Furthermore, a positive pitch angle θ implies a bow-down rotation.

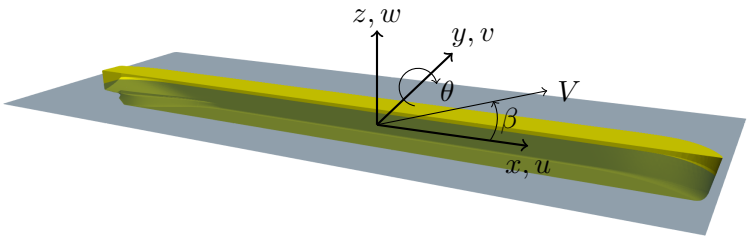

Figure 4. Positive orientation of the relevant ship motions and velocities.

3.4 Definition of the hull loads and motions

The quantities of interest in the numerical study are the surge force (X), the sway force (Y) and the yaw moment (N), as well as the sinkage (z) and the trim (θ) of the ship. Their positive orientation can be deduced from figure 4. Combined, this set of variables is generally the minimum required in the subsequent construction of mathematical (fast-time) models for pure drift manoeuvres. In order to compare hydrodynamic loads at different speeds and dimensions, the hull forces presented in this paper are made dimensionless following the definitions below:

$$X' = \frac{X}{1/2\rho V^2 L_{pp} T}, \qquad Y' = \frac{Y}{1/2\rho V^2 L_{pp} T}, \qquad N' = \frac{N}{1/2\rho V^2 L_{pp}^2 T}, \tag{5}$$

with X, Y and N the hull loads, ρ the fresh water density, T the mean draught in undisturbed water, V the reference ship speed and L_{pp} the ship's length between perpendiculars. Furthermore, the sinkage is scaled with the draught at rest T.

3.5 Numerical settings and boundary/initial conditions

For the spatial discretisation of the momentum equations, a second-order (limited) scheme (Waterson and Deconinck, 2007) is employed, while for the turbulence equation a first-order upwind scheme is used for improved robustness. The linear systems that stem from the momentum and turbulence equations are solved using a GMRES solver with a Block Jacobi preconditioner, and the pressure system is solved using a preconditioned Conjugate Gradient method. The nonlinear set of equations is linearized using Picard iteration and subsequently solved in a segregated manner using a first order implicit time integration method. The k-$\sqrt{}$kL model (Menter et al., 2006) is mostly used for the (RANS) turbulence equations although some computations are done with the k-ω SST model (Menter, 1994) for comparison. The time step in the unsteady simulations is chosen to keep the Courant number roughly below five for robustness.

The free surface is modelled as an essential part of the algorithm to determine the squat during the calculation. An algebraic Volume-of-Fluid method is used to represent the air-water interface (Klaij et al., 2018).

The rectangular computational domain has dimensions $9L_{pp} \times 2.59L_{pp} \times 1.29L_{pp}$ and matches the width of the basin. Inflow and outflow conditions are applied on the boundaries normal to the center line, and on the top boundary of the domain the pressure value is fixed. Both side boundaries and the bottom are modelled as moving walls with velocity equal to the (negative) sailing speed. The ship surface finally is modelled as a no-slip wall.

The sailing velocity is used throughout the domain as initial condition, combined with the hydrostatic pressure. Decaying damping regions, in which any fluctuations in velocity or free surface height are forced to the undisturbed flow solution, are initially placed upstream from the ship to mitigate the impulsive start of the simulation.

4 COMPARISON BETWEEN CFD AND EXPERIMENTAL RESULTS

In this section, hydrodynamic loads and squat motions predicted in CFD calculations are compared with experimental results.

4.1 Hydrodynamic loads

Figure 5 shows the non-dimensional hydrodynamic forces as well as the yaw moment on the hull at various speeds for three water depths. The experimental results are obtained at intervals of 2 degrees.

Overall, it can be seen that experimental and numerical hull forces follow the same trends as a function of the drift angle. The experimental hull forces increase as the water level decreases, and this is well captured by the simulations. This is particularly noticeable in the sway force and yaw moment, where shallow-water effects are more tangible. In addition, the experimental hull forces evidence a certain speed dependence, especially in the shallowest case ($h/T = 1.2$) where the speed difference is 20%. This can be best seen in the sway force and yaw moment, in particular at the highest drift angle of 6 degrees. The increase in non-dimensional hull force as the speed increases is highly related to the increase of squat (see next section). Similarly, a speed dependency can also be observed in the CFD calculations.

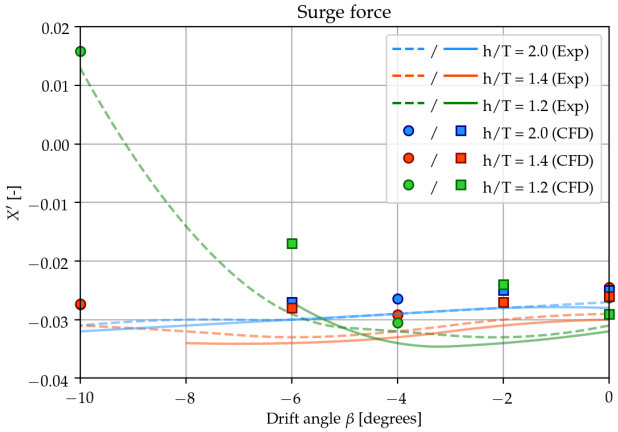

(a) Surge force for varying UKC.

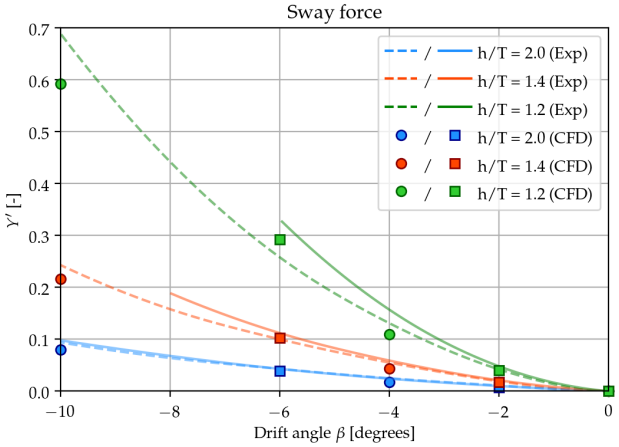

(b) Sway force for varying UKC.

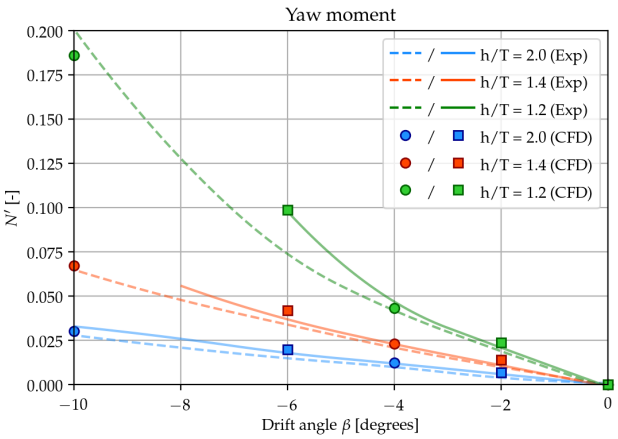

(c) Yaw moment for varying UKC.

Figure 5. Hull loads in pure drift motion: numerical (markers) and experimental results (lines). The continuous lines and the square markers represent the cases with constant speed ratio V/V_{c_r}, the dashed lines and the round markers represent the case with constant speed V for all water depths.

The largest discrepancy is found in the surge force where relative errors up to 40% are found. Because of their small magnitude, measurement errors in the experiments could become significant and pollute the results. In addition, the relatively low test speed may induce scale effects on the surge force, which is highly dependent on friction and Reynolds number. The flow around the ship model may not be fully turbulent, while a flow field that contains both laminar and turbulent regions cannot be captured numerically using RANS modelling. From a computational point of view, the resistance, unlike the drift force and the yaw moment, is highly dependent on the frictional contribution of the flow which remains difficult to predict well due to its dependence on the turbulence model used. Although unlikely considering the drift angles used, flow separation is generally also not well captured by RANS methods and can be another source of discrepancy with the experimental results. Finally,

the CFD computations are performed on a computational mesh with a cell density that balances the desired accuracy with the computing time required to obtain a solution. It is possible that the flow phenomena in shallow water require more mesh resolution to capture the complex physics around the vessel. Subsequent grid refinement studies are mandatory to investigate this discrepancy further.

4.2 Squat

The simulations of the cases with constant speed ratio were carried out allowing two degrees of freedom to the hull: heave and pitch. This approach enables a more realistic representation of a ship sailing at forward speed, as it dynamically sinks and trims until it reaches an equilibrium. This becomes even more important in shallow water, when the squat effect enhances dynamic trim and sinkage experienced by the sailing ship.

Figures 6a and 6b present the average sinkage and trim identified under the different conditions of pure drift motion tests for both CFD computations and basin tests. Sinkage is made non-dimensional using the static draught T.

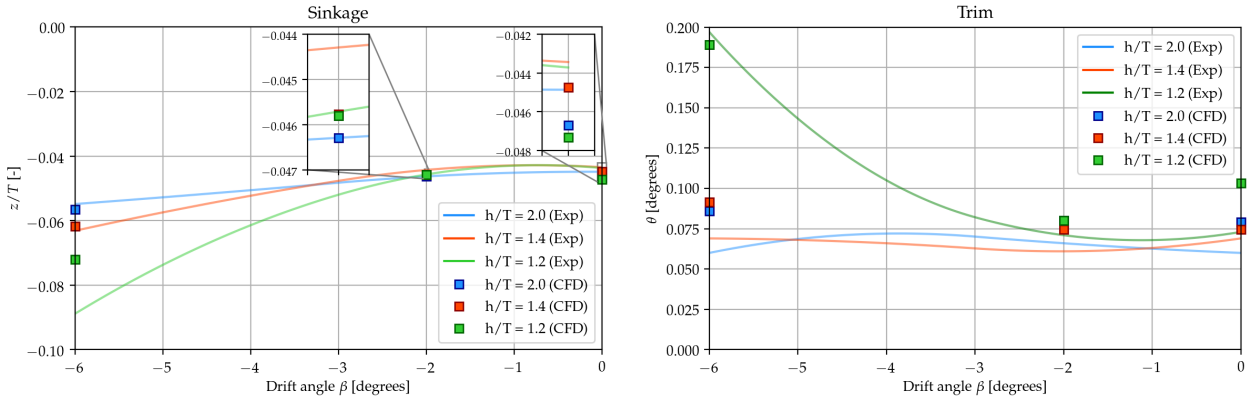

(a) Sinkage for varying UKC.

(b) Trim angle for varying UKC.

Figure 6. Dependance of the squat on drift angle: numerical (markers) and experimental results (lines).

It can be seen that experimental and numerical results show similar overall trends: increasing trim and sinkage as the drift angle increases and the water level decreases. Sinkage values are in particular very consistent between the two methods, with the exception at a drift angle of 6 degrees for a water depth-to-draught ratio of 1.2, where CFD underpredicts the sinkage observed during the model tests by nearly 20%.

Trim results evidence that this particular ship always trims with the bow down. The angles are small, in the order of 0.08 degrees, which is close to the limit of the measuring equipment in the basin. Nevertheless, both methods indicate comparable trends. It is interesting to find that CFD tends to slightly overpredict the trim (bow down) compared to the experimental measurements.

Local deformation of the computational mesh is used to model trim and sinkage (both dynamic and imposed). It was found that for shallow water cases the mesh deformation occasionally becomes challenging due to the proximity of the bottom wall. Boundaries of the domain (including the ship) effectively impose constraints on how the internal volume mesh is allowed to deform. The CFD input contains various parameters to control the deformation, and it was found that the resulting deformed mesh is quite sensitive to the input. Insufficiently accurate deformation can lead to divergence of the simulation, but to reach sufficient accuracy the calculation becomes costly. It remains a challenge to deform the mesh correctly and efficiently in shallow-water cases, and this topic is among others to be further investigated in future developments of ReFRESCO.

4.3 Challenges

Reproducing experimental pure drift motions in shallow (and confined) water by means of CFD calculations proves to be a complex endeavour, as the uncertainties introduced by the numerical reproduction of a real-life configuration are added to the uncertainties inherent to the basin tests. Consequently, it is important to consider the following challenges when attempting to reproduce model tests by means of CFD.

Low test speeds The relatively low velocities used paradoxically lead to increased complexity in the CFD computations. By default, the flow in numerical simulations is modelled as fully turbulent on meshes that are too coarse to fully resolve all its characteristics. During the experiments, on the other hand, the low velocity can lead to regions around the ship with laminar flow while other regions experience a turbulent flow. The difference in physical behaviour (shear stress on the hull, flow separation, etc.) cannot be simultaneously captured by CFD and this can lead to differences between the measured and computed hull forces, in particular in surge.

Choice of turbulence model Because of the low sailing velocities, the frictional contribution to the hydrodynamic loads is relatively high, particularly for the surge force. As the numerical computations assume turbulent flow, the choice of turbulence model directly influences the shear stress on the hull and therefore the surge force. The variety of turbulence models available lead to significant differences (Pereira et al., 2017), which should be kept in mind.

Accuracy of squat measurements In most cases, the inland ship experienced a limited trim and sinkage. Consequently, values registered during the experiments, and used as input in the simulations, are close to the measurement accuracy in the case of the trim. Comparison of dynamic trim values should then be used with care.

Residual basin current During the model tests, each run is followed by a waiting time (from 15 to 25 minutes) to limit the residual current in the tank induced by the towing of the model back and forth. However, residual currents persist a long time in extremely shallow water, and may not have completely disappeared after the waiting time, while calculations model perfectly still water. A recent investigation with the same ship model showed however that this effect was negligible.

Accuracy and smoothness of the basin geometry The bottom of the basin is considered relatively flat and smooth, which is sufficient for most test programs. Nevertheless, the roughness of the tank bottom cannot be disregarded (considering keel clearance is less than 4 cm for $h/T = 1.2$). The same holds for the planarity and smoothness of the towing structure that is used in the experiments.

5 CONCLUSIONS

Comparison with experimental results shows that CFD is able to reproduce the distinct trends in hull forces and squat for small drift angles in shallow water using standardised procedures and meshes. While numerical and experimental results are well aligned in mildly shallow water, differences grow as the under-keel clearance decreases further. This may indicate higher uncertainties or modelling errors, which are inherent to the methods considered. Possible sources explaining these discrepancies have been pointed out, and based on these findings it is recommended to perform a dedicated investigation to quantify uncertainties, both in CFD and experiments, for a conscientious quantitative comparison.

References

Maritime Research Institute Netherlands, ReFRESCO web page. https://www.marin.nl/facilities-and-tools/software/refresco. Accessed: 01-04-2021.

J. Brouwer, J. Tukker, Y. Klinkenberg, and M. van Rijsbergen. Random uncertainty of statistical moments in testing: Mean. *Ocean Engineering*, 182:563–576, 2019.

P. Crepier. Ship resistance prediction: verification and validation exercise on unstructured grids. In *MARINE VII: proceedings of the VII International Conference on Computational Methods in Marine Engineering*, pages 365–376. CIMNE, 2017.

C.M. Klaij, M. Hoekstra, and G. Vaz. Design, analysis and verification of a volume-of-fluid model with interface-capturing scheme. *Computers & Fluids*, 170:324–340, 2018.

F.R. Menter. Two-equation eddy-viscosity turbulence models for engineering applications. *AIAA journal*, 32(8):1598–1605, 1994.

F.R. Menter, Y. Egorov, and D. Rusch. Steady and unsteady flow modelling using the k-$\sqrt{}$kl model. In *Turbulence Heat and Mass Transfer 5. Proceedings of the International Symposium on Turbulence Heat and Mass Transfer*. Begel House Inc., 2006.

F.S. Pereira, L. Eça, and G. Vaz. Verification and validation exercises for the flow around the kvlcc2 tanker at model and full-scale reynolds numbers. *Ocean Engineering*, 129:133–148, 2017.

T.C.S. Rendall and C.B. Allen. Efficient mesh motion using radial basis functions with data reduction algorithms. *Journal of Computational Physics*, 228(17):6231–6249, 2009.

K. Römisch. *Empfehlungen zur Bemessung von Hafeneinfahrten*. Technische Universität Dresden, 1989.

S.L. Toxopeus, C.D. Simonsen, E. Guilmineau, M. Visonneau, T. Xing, and F. Stern. Investigation of water depth and basin wall effects on KVLCC2 in manoeuvring motion using viscous-flow calculations. *Journal of Marine Science and Technology*, 18(4):471–496, 2013.

N.P. Waterson and H. Deconinck. Design principles for bounded higher-order convection schemes–a unified approach. *Journal of Computational Physics*, 224(1):182–207, 2007.